Numerical Study of Three-Dimensional Shock Control Bump Flank Effects on Buffet Behavior

R. Mayer, D. Zimmermann, K. Wawrzinek, T. Lutz, and E. Krämer

Abstract Originally developed as a flow control device Shock Control Bumps (SCB) reduce wave drag of an aircraft wing at off-design in transonic speed effectively. Recently, another field of application for such bumps has been studied, namely the delay and alleviation of buffet, an unsteady shock motion due to continuous flow separation and re-attachment at the rear part of the airfoil. In principle the idea of buffet alleviation is the use of SCB as a sort of 'smart' vortex generator. Considerable effort has been undertaken to link geometrical bump features to buffet affecting flow characteristics. In this paper a parametric study on the influence of flank shape of a three-dimensional wedge-shaped SCB on its performance and buffet behavior is presented. It has been found that performance as well as buffet behavior can be improved by optimization of the bump flanks. The study shows that length of front and rear flank should be increased up to given constraints (e.g. flaps on a wing or inserts for a wind tunnel model) and a narrow front and wide rear flank increase $c_{L,max}$ and damp lift oscillations at buffet onset.

1 Introduction

First introduced by Ashill, Fulker and Shires [1] in 1992, Shock Control Bumps (SCB) are a passive method of flow control in transonic flow regime with the objective of reducing wave drag. Accurately designed, wave drag of an airfoil resp. a wing is negligible at design conditions. However, increasing angle of attack or Mach number leads to a strong increase of wave drag, referred to as transonic drag rise. This drag rise normally reduces flight performance significantly. Therefore, SCBs can help to improve performance at airfoil/wing off-design conditions (see e.g. [13]).

Recent studies focus on another field of application for SCBs, namely the alleviation of the buffet phenomenon. Buffet limits flight Mach number and maximum lift of an airliner. It is characterized by a continuously separation and

R. Mayer (✉) • D. Zimmermann • K. Wawrzinek • T. Lutz • E. Krämer
Institute of Aerodynamics and Gas Dynamics, University of Stuttgart, Stuttgart, Germany
e-mail: r.mayer@iag.uni-stuttgart.de; zimmermann@iag.uni-stuttgart.de; wawrzinek@iag.uni-stuttgart.de; lutz@iag.uni-stuttgart.de; kraemer@iag.uni-stuttgart.de

W.E. Nagel et al. (eds.), *High Performance Computing in Science and Engineering '15*, DOI 10.1007/978-3-319-24633-8_32

re-attachment of the boundary layer, resulting in shock and lift oscillations. It has been shown [2, 3] that SCBs can have a double benefit by reducing wave drag at off-design conditions and increasing lift coefficient at which buffet indicating lift oscillations first occur. In general, the intention is to use SCBs as a novel class of 'smart' vortex generators and thereby introducing stream-wise vortices in the flow. These vortices act as a sort of boundary layer control and prevent the flow downstream of the bump from separating. The precise mechanism by which the vorticity is generated by the bump is still unsolved and subject of current research (e.g. [3, 6, 10]). Recent publication [7] indicates that the span-wise pressure gradient present on the front flank of a SCB is strongly related to the vorticity generated by the bump. In addition, the rear flank design is correlated to flow separation present on the SCB. Bruce and Colliss [5] state that a wider tail can be beneficial at off-design conditions by reducing re-acceleration over the crest to obtain a reduction in the extent of local separation around the SCB crest region.

This paper presents a parametric study analyzing the effect of front and rear flank shapes of a generic wedge-shaped three-dimensional SCB on performance and buffet behavior of the airfoil. First, the numerical methods used as well as the baseline airfoil and bump design are presented. Then, the effect of flank shape on different parameters like aerodynamic efficiency, maximum lift coefficient and lift oscillations at buffet onset are discussed in detail. Finally, trends for the flank shape of buffet alleviating bumps are derived.

2 Numerical Methods

2.1 Flow Solver

FLOWer [15] is a block-structured RANS solver developed by German Aerospace Center (DLR) to meet the demands of aircraft aerodynamics. In order to determine a suitable setting for buffet simulations, this flow solver has been validated using the well documented OAT15A airfoil. The buffet characteristics of this airfoil have been analyzed excessively in wind tunnel experiments [12], providing a valuable database for buffet calibration of flow solver settings. Experimental buffet onset has been found at an angle of attack (AoA) of $\alpha = 3.25°$ with a buffet frequency of $f_{\text{buffet}} \approx 70\,\text{Hz}$. Three-dimensional (U)RANS simulations have been carried out with the settings discussed in Sect. 2.2 to analyze the buffet behavior of the OAT15A airfoil numerically. Out of a range of different turbulence models tested (Spalart-Allmaras (SA), SA-Edwards, SA-salsa, SST-k-ω and LEA-k-ω) the *Strain Adaptive Formulation of Spalart-Allmaras One-Equation Model* (SA-salsa) performed best, finding buffet onset (here defined as the lowest angle of attack at which URANS simulations capture lift oscillations) at $\alpha = 3.2°$ with an accuracy of $\Delta\alpha = 0.1°$. The buffet frequency was computed to $f_{\text{buffet}} \approx 73\,\text{Hz}$ which is in excellent agreement with the experimental results.

2.2 Computational Set-up

For all flow simulations, the cell-centered approach has been applied. The computations have been carried out with a central scheme (according to Jameson) for spatial discretization. Temporal discretization is achieved with a central Runge-Kutta scheme. For convergence acceleration, a 3-stage sawtooth-V-cycle multi-grid has been applied and the residual has been smoothed with variable coefficients according to Swanson. For CFL number varying between 1.0 and 7.5, computations have been carried out up to a residual of less than $1.0e^{-6}$. Based on the results from Sect. 2.1, 1-equation turbulence model SA-salsa has been used.

In order to prevent laminar shock-boundary-layer interactions in the numerical simulations and thereby reduce numerical robustness considerably, transition is tripped at 35 % of chord, just upstream of the most upstream shock location in case of buffet.

For URANS simulations, a dual time stepping scheme with a time step size of $5.7e^{-5}$ s has been applied, resolving an estimated buffet frequency of 70 Hz with approximately 250 time steps as recommended by several authors [3, 17]. The mean values as well as buffet characteristics have been determined by analyzing eight buffet cycles in fully established flow.

2.3 Grid

All simulations presented in this paper base on structured H-C type, multi-block meshes with boundary layer refinement which have been generated script-based, ensuring consistently high quality meshes for each SCB configuration and thereby reducing the grid influence on the solution to a minimum. A grid convergence study for those meshes can be found in [14]. Nevertheless, a short overview of the mesh topology shall be given here.

For the three-dimensional simulations the grid around the airfoil (see Sect. 3.1) has been extruded 30 % of chord length in span-wise direction. The far-field extends to 50 chord lengths from the airfoil. A boundary layer refinement of the grid leads to a first cell height of $y_1^+ \approx 0.8$. For better physical agreement with experimental results the scripts for automated mesh generation from [14] have been adapted to blunt trailing edge airfoils. In total, the meshes consist of approximately 6.0 million cells with 352 cells around the airfoil, 32 cells on the trailing edge and 64 cells in the wake in stream-wise direction. In accordance to [14] the number of span-wise cells has been set to 120.

3 Baseline Geometry

All calculations presented in this paper base on the OALT25 airfoil, further discussed in Sect. 3.1. Corresponding to the design condition of this airfoil, all simulations have been carried out for $Re = 13e^6$ and $Ma = 0.73$. Stagnation temperature has been set to $T_{st} = 300\,\mathrm{K}$.

3.1 Airfoil

As baseline airfoil OALT25 developed by ONERA has been used. Reference condition of this airfoil are $Ma = 0.73$, $Re = 13e^6$ and $AoA = 1.0°$. With a relative thickness of 12.18 % and a trailing edge thickness of 0.5 % of chord, this transonic airfoil has been designed for delayed transition. In the S3Ch wind tunnel at ONERA, the boundary layer remains laminar up to the shock at around 60 % of chord.

3.2 Shock Control Bump

In accordance to previous studies by Bogdanski [3], who analyzed the buffet behavior of SCBs designed for drag reduction at high lift coefficients, a Wedge-SCB has been optimized in height and position for minimum drag coefficient as a first step towards a buffet alleviating bump. Figure 1 shows the optimized Wedge-SCB on the suction side of the airfoil placed near the shock foot. The bump parameterization allows for detailed adaption to the flow condition but has also a rather simple shape which is essential for parametric studies on geometrical effects. The upstream flank, the crest plateau as well as the rear flank are plain. The side flanks are modeled by a 4th order polynomial using the base point (intersection between bump and airfoil), the top point (intersection between side flank and mid-section), the side flank angle at the base point as well as the curvature (4th derivative of polynomial) at the top point at each stream-wise position. The height of the bump refers to the crest plateau of the bump.

Using a SIMPLEX algorithm, the bump parameters have been optimized for minimum drag coefficient. The bump design point (BDP) has been chosen carefully based on an elaborate analysis of the baseline airfoil. At $\alpha_{BDP} = 1.7°$ respectively $c_{L,BDP} \approx 0.8$, MSES simulations [9] indicate that wave drag contributes with around 17 % to total drag, offering sufficient potential for drag reduction by SCB. In addition, an analysis of shock location for an AoA range between airfoil design point and buffet onset revealed a downstream movement of the shock with increasing AoA up to $\alpha \approx 2.5°$. For higher AoA the shock moves upstream again. Since bump position in relation to shock location affects the performance of the bump

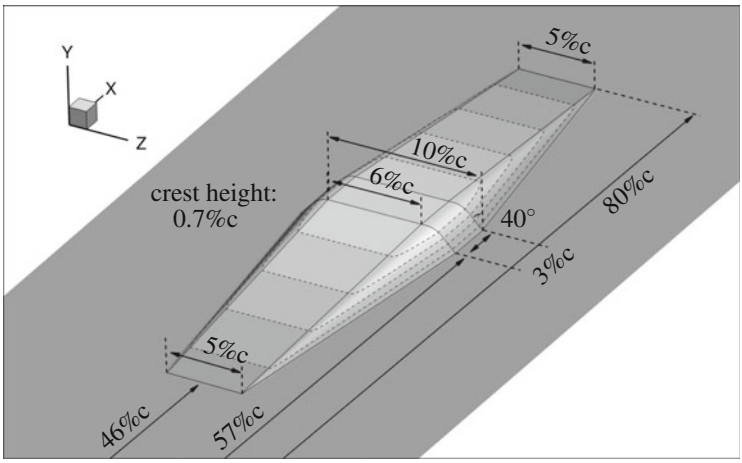

Fig. 1 Baseline Wedge-SCB with parametrization

significantly, the design AoA of the bump has been chosen to have the same shock location as at buffet onset.

At bump design condition, this bump reduces drag by 8.3 % leading to an improved aerodynamic efficiency of 9.2 %. A well known disadvantage of SCBs is their performance deterioration at bump off-design conditions. At design condition of the airfoil drag is increased by 20.7 %, reducing aerodynamic efficiency by 19.1 %.

In contrast to studies by Bogdanski [3], this baseline SCB does not improve the buffet behavior of the OALT25. The reason is a significant difference between highest AoA ($\alpha = 2.4°$) at which RANS simulations converged and buffet onset AoA ($\alpha = 3.4°$), not allowing for bump optimization close to buffet onset. Obviously, URANS simulations would be more appropriate for buffet alleviating bumps but these simulations are to costly for three-dimensional bump optimization.

4 Influence of Flank Shape

As found by other researchers [5, 6] the flanks of the bump affect the buffet behavior. Colliss [7] found that the vorticity generated by the bump strongly depends on the maximum span-wise pressure gradient on the front flank of the bump. Thinking of buffet alleviating bumps as a kind of 'smart' vortex generators it seems to be beneficial to maximize generated vorticity in order to strengthen the boundary layer downstream of the bump and thereby delaying separation. In addition, the rear flank design has found to be correlated to flow separation on the bump [5]. Since any kind of flow separation weakens the boundary layer downstream it can be assumed that a minimization of flow separation on the bump will help to delay buffet onset.

Table 1 Parameter space for flank variation

Setup	FFL (%c)	FFW (%c)	RFL (%c)	RFW (%c)	FFLf	FFWf	RFLf	RFWf
Baseline	11	5	20	5	1.0	1.0	1.0	1.0
FF1	5.5	2.5	20	5	0.5	0.5	1.0	1.0
FF2	5.5	10	20	5	0.5	2.0	1.0	1.0
FF3	5.5	15	20	5	0.5	3.0	1.0	1.0
FF4	11	2.5	20	5	1.0	0.5	1.0	1.0
FF5	11	10	20	5	1.0	2.0	1.0	1.0
FF6	11	15	20	5	1.0	3.0	1.0	1.0
RF1	11	5	10	2.5	1.0	1.0	0.5	0.5
RF2	11	5	10	10	1.0	1.0	0.5	2.0
RF3	11	5	10	15	1.0	1.0	0.5	3.0
RF4	11	5	20	2.5	1.0	1.0	1.0	0.5
RF5	11	5	20	10	1.0	1.0	1.0	2.0
RF6	11	5	20	15	1.0	1.0	1.0	3.0

FFL(f) front flank length (factor), *FFW(f)* front flank width (factor), *RFL(f)* rear flank length (factor), *RFW(f)* rear flank width (factor)

The precise mechanism by which vorticity is generated by the bump is still unsolved and subject of current research (e.g. [3, 6, 10]). The objective of the present paper is to link geometry parameters (such as flank length and width) to aerodynamic performance and buffet behavior of the bump.

In total, six different front flank (FF) shapes and six different rear flank (RF) shapes have been analyzed. Table 1 gives an overview of the parameter space. It has to be noted that only one flank (front or rear) was modified at a time.

4.1 Flank Parameter

As mentioned in Sect. 4 the maximum span-wise pressure gradient on the front flank of the bump as well as flow separation on the bump seem to be related to the buffet behavior. Therefore, the effect of flank shape on those two parameters shall be analyzed first.

Figure 2 shows the maximum span-wise pressure gradient extracted from a slice at stream-wise mid of front flank. The contour gives a good tendency for the effect of front and rear flank shape on this parameter. In general, a short and very wide front flank produces large pressure gradients. Compared to the baseline bump (blue square), the pressure gradient can be nearly sextupled. The shape of the rear flank has obviously no effect on the pressure gradient on the front flank.

Flow separation is determined by analyzing the skin friction coefficient c_f. For two-dimensional simulations $c_{fx} < 0$ is a sufficient criterion. In case of three-dimensional simulations the situation is more complex since cross flow has to be

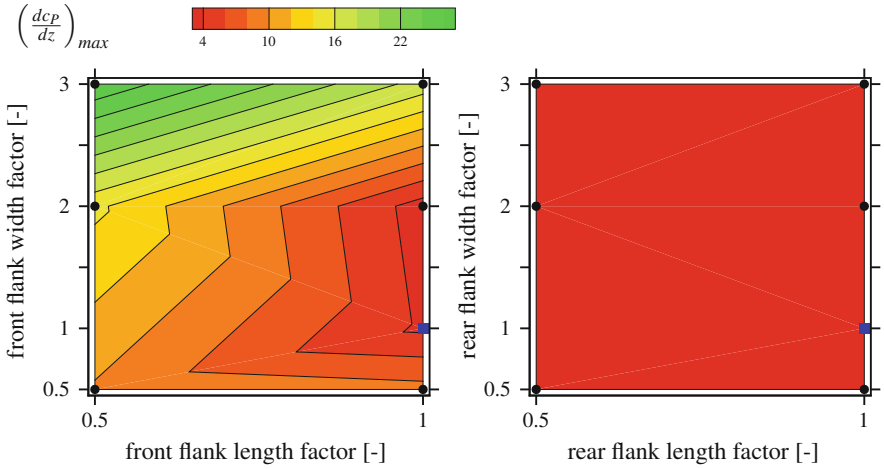

Fig. 2 Maximum span-wise pressure gradient on front flank at $Ma = 0.73$ and $AoA = 1.7°$ (bump design condition)

considered. For this reason Illi [11] used the 'combined' skin friction coefficient $c_{f\Phi}$.

$$c_{f\Phi} = \frac{2}{\pi} \tan^{-1}\left(sgn(c_{fx}) \cdot \frac{\sqrt{c_{fx}^2 + c_{fy}^2}}{|c_{fz}|} \right) \tag{1}$$

As a measure of the direction of surface skin friction, $c_{f\Phi}$ equals 1 for attached flows and -1 for separated flows. The range between -1 and 1 indicates dominating cross flows. In order to evaluate the percentage of separated flow on the bump, $c_{f\Phi}$ has been averaged in an area between 35 % and 80 % of chord in stream-wise direction over the entire span of 30 % of chord of the wing section.

As found by other authors [5] the rear flank has a stronger effect on flow separation compared to the front flank, see Fig. 3. Generally, a longer flank reduces stream-wise pressure gradients and thereby prevents the boundary layer from early separation. Considering the flank widths, wider bumps are beneficial with respect to flow separation.

4.2 Bump Performance

Performance of the bump is assessed by evaluating aerodynamic efficiency. Figure 4 shows the effect of flank shape on aerodynamic efficiency at bump design condition and Fig. 5 at airfoil design condition, respectively. First of all, it is interesting to

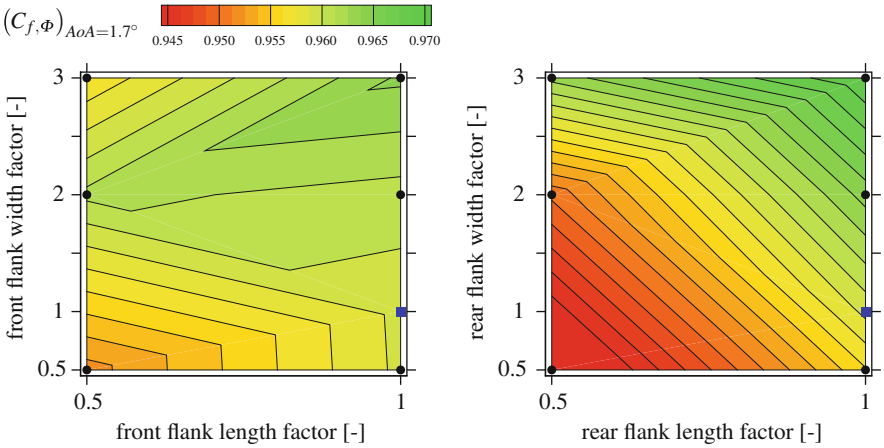

Fig. 3 Skin friction coefficient $C_{f,\Phi}$ at $Ma = 0.73$ and $AoA = 1.7°$ (bump design condition)

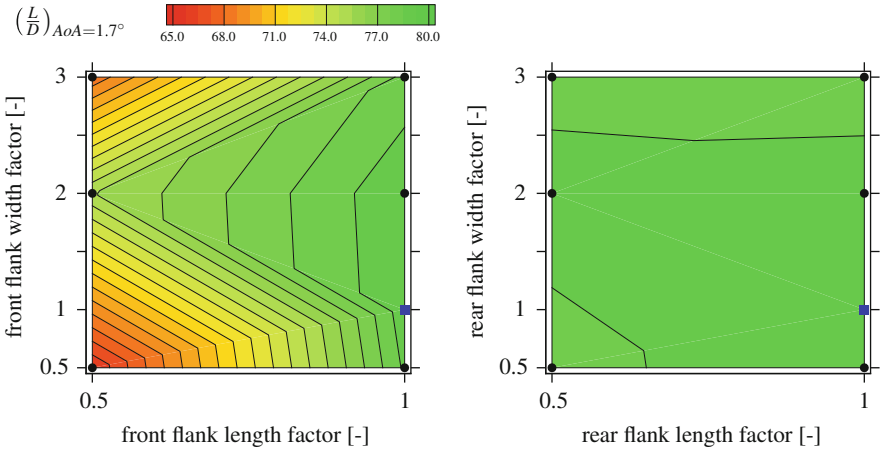

Fig. 4 Lift-to-drag ratio at $Ma = 0.73$ and $AoA = 1.7°$ (bump design condition)

see that the rear flank width does not affect aerodynamic efficiency at bump design condition whereas it affects performance at bump off-design conditions. The main reason for that is the positioning of the bump in relation to the shock position. At bump design condition the shock foot is on the front flank close to the crest. At bump off-design condition a double-shock systems establishes. The downstream/second shock occurs at the rear flank. Here, a wider flank further re-accelerates the flow and therefore increases shock strength, leading to a performance deterioration.

As written in Sect. 3.2 the bump has only been optimized in height and position. For all other parameters (like flank width) default parameters have been used. For

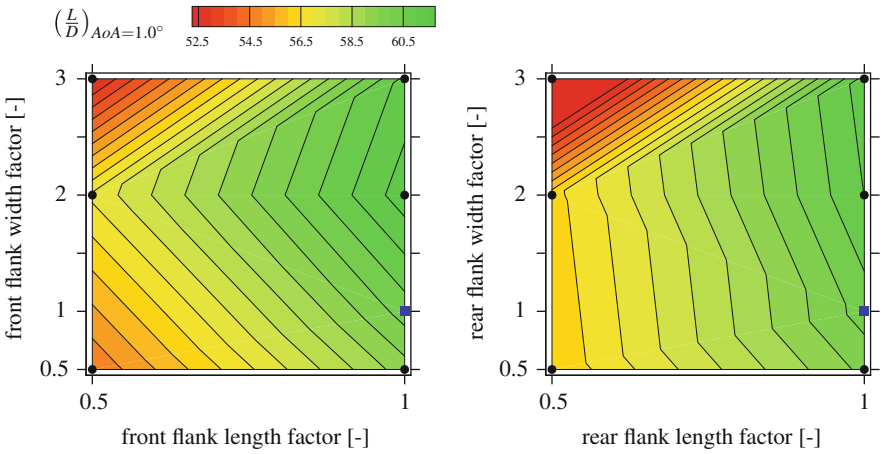

Fig. 5 Lift-to-drag ratio at $Ma = 0.73$ and $AoA = 1.0°$ (airfoil design condition)

this reason there is a slight increase of aerodynamic efficiency for wider front flanks compared to the baseline bump.

As a general trend, long front and rear flanks are beneficial with respect to aerodynamic efficiency. Concerning the width there seems to be an optimum at widths close to or equal to the width of the mid-section of the bump (here 10 %c).

4.3 Buffet Behaviour

In order to assess the buffet behavior, two flow characteristics have been analyzed. From an industrial point of view, maximum lift coefficient (Fig. 6) and strength of lift oscillations at buffet onset (Fig. 7) are most important. For analysis of lift oscillations, eight buffet cycles in a fully established flow field have been analyzed.

In general, long front flanks provide a higher maximum lift coefficient. This corresponds to the findings from Sect. 4.2 that an increased flank length is beneficial for the boundary layer state. Considering flank width there is a clear trend towards narrow front and wide rear flanks. One explanation might be an induced 'extra' lift, generated by the vortices emerging from the side flanks of the bump.

Comparable to maximum lift coefficient, longer flanks seem to reduce the root mean square of lift oscillations at buffet onset, see Fig. 7. However, the main parameter affecting lift oscillations seems to be the flank width. Here, rather extreme front flank widths perform better. This correlates to the results of the span-wise pressure gradient, verifying the findings of [7]. Considering rear flank width, wider bump tails reduce lift oscillations at buffet onset.

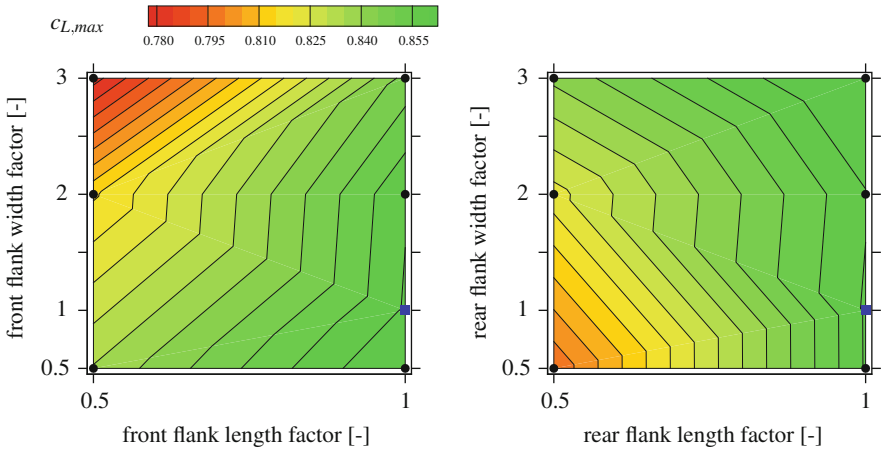

Fig. 6 Maximal lift coefficient at $Ma = 0.73$

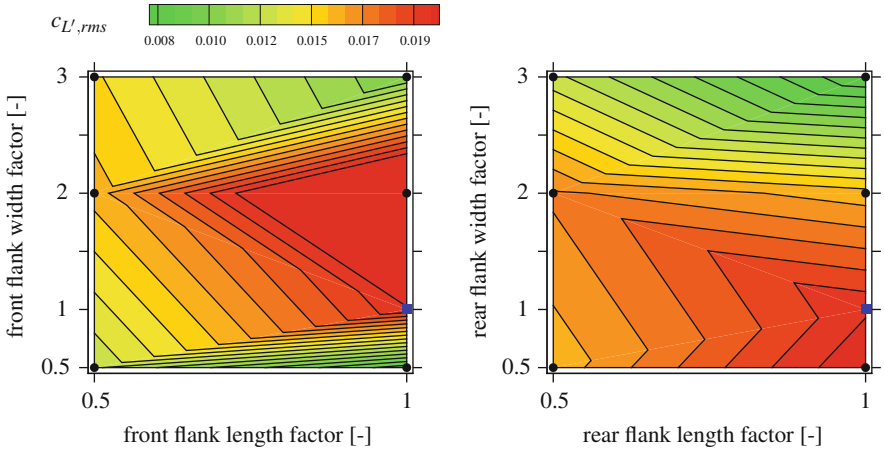

Fig. 7 RMS of lift oscillations at buffet onset ($Ma = 0.73$)

5 Trends for Optimal Flank Shape

Considering the results presented in Sect. 4 trends for optimal flank shape of buffet alleviating bumps can be derived. Overall, reducing the length of the flanks worsens both, performance and buffet behavior. Purely optimizing the bump for good buffet behavior ($c_{L,max}$, $c_{L',rms}$) leads to a narrow front and a wide rear flank shape. In contrast to that most desirable would be a 'double benefit bump', alleviating buffet *and* improving performance at airfoil/wing off-design conditions. Including the effect of flank shape on aerodynamic efficiency (see Sect. 4.2), the 'optimum'

flank shape slightly changes. Especially a 'too narrow' front flank deteriorates the performance.

Concluding, performance and especially buffet behavior of the baseline bump can be improved by modified flank shapes. Both, front and rear flank have only to be adapted in width, not in length. In fact, a further extension in stream-wise direction ('longer flanks') seems to be beneficial. But normally the bumps' length is a highly restricted parameter (e.g. by flaps, spoiler, bump inserts for wind tunnel measurements) not allowing for considerably increase of flank length. The front flank width should by slightly reduced by a factor of $0.5 < FFWf < 1$. Width of the rear flank should be increased up to the boundary of the analyzed parameter space ($RFWf \simeq 3$).

In addition, a comparison with flank parameters in Sect. 4.1 shows that both, maximum span-wise pressure gradient on the front flank as well as low separation on the bump shape are suitable design parameter for buffet bump optimization.

6 Computational Resources

In the near future several buffet alleviating bumps will be analyzed with higher order methods (e.g. DES) resulting in considerably larger meshes. It has not been decided yet about the flow solver to be used. Besides the structured flow solver FLOWer which has been used in the present study, the unstructured flow solver TAU (also developed by DLR) is up for discussion. The advantages of this solver are its excessive validation for buffet simulations (e.g. [11]) and significantly more implemented methods.

For numerical costly simulations, performance of the flow solver on the high performance cluster is very important for minimization of computational effort. Therefore, a scaling test on the CRAY XC40 was performed for both flow solvers to ensure an optimum utilization of resources. In this paper, the test results of the scaling tests applying the flow solver TAU release version 2014.2.0 are presented. A detailed description of the respective scaling test applying the structured flow solver FLOWer can be found in [16]. The scaling tests includes both, a weak scaling test and a strong scaling test, and are based on a generic test case. These test cases consist of a cubic mesh containing 33.5 million cells (33.9 million points) for the strong scaling test and 32,768 cells per core for the weak scaling test, respectively. The boundaries of the cube are set to far field conditions. For preprocessing of the TAU test cases, the native partitioner, included in the TAU software package, was applied. The usage of the new parallel initial partitioner was switched off and the old one was applied, which computes the partitions in a parallel matter but stores initially the entire grid on process 0 [8]. For all simulations, a central differences scheme was used, including a second order scheme for spatial discretization and a LUSGS scheme for backward Euler-time integration. The two-equation model k-ω was applied for turbulence modeling.

Three different compiler settings were tested to compile the TAU Code on the CRAY XC40: CRAY 8.3.8, GNU 4.9.2 and INTEL 15.0.2.164. Based on results of prior scaling tests on the CRAY XE6, the compiler PGI was excluded from the present scaling test due to its poor performance results [4]. For each compiler setting, the respective NetCDF version 4.3.2 and MPICH2 version 7.1.2 was included.

During all scaling tests, the so-called 'Real-time' of the solver TAU was logged to achieve scalable results. 'Real-time' is defined as the time from the first to the last iteration of the process and includes time the process spends blocked in case if it is waiting for other processes to complete. The initialization process and the write out time are not taken into account. For all tests, a number of 1000 Iterations have been calculated.

Starting with the weak scaling test, this test consists of several mesh sizes and process numbers in such a way that every process treats 32,768 cells, independent of the process count. A range from 128 to 3072 domains was tested. First of all, wall-clock time of the preprocessing tools 'subgrids' and 'preprocessing' of the TAU code were gathered and are presented in Fig. 8a and b, respectively. This data was collected for the CRAY-compiled version of the TAU code and partly complemented by the other two compiler versions. Both figures indicate a nearly linear increase of the logarithmic time plotted against the logarithmic number of cores. There are no major differences observable between the three tested compiler versions.

In the second place, the 'real-time' of the solver TAU was measured for all compiler version installed. To minimize any dependency on the allocated cores for the respective job, all tests are repeated three times. The results are given in Fig. 9a–c for each compiler version, respectively. Here, the 'real-time' for 1000 iterations is plotted against the number of cores.

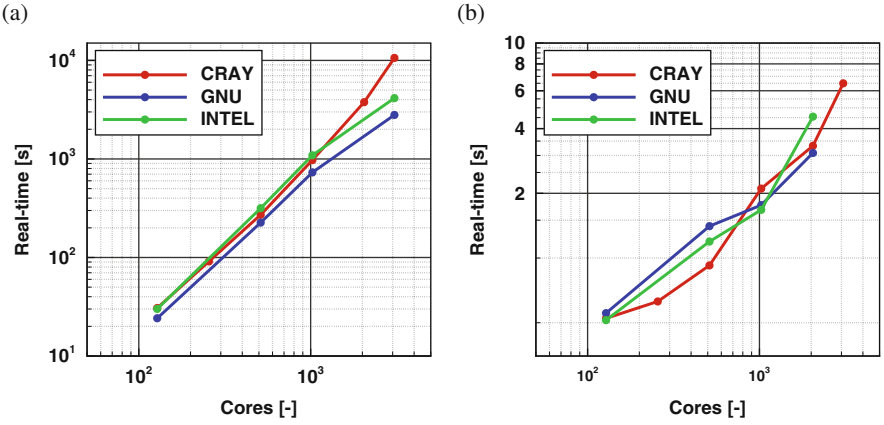

Fig. 8 'Real'-time of the preprocessing tools; CRAY-compiled version of TAU version 2014.2.0. (**a**) 'Subgrids' tool. (**b**) 'Preprocessing' tool

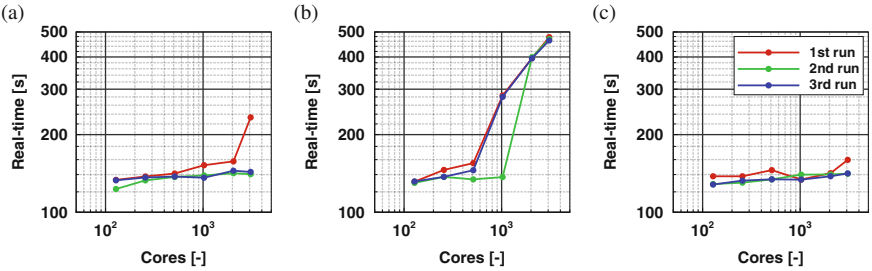

Fig. 9 'Real'-time results for different compilers; TAU version 2.2.0. (**a**) CRAY-compiled version. (**b**) GNU-compiled version. (**c**) INTEL-compiled version

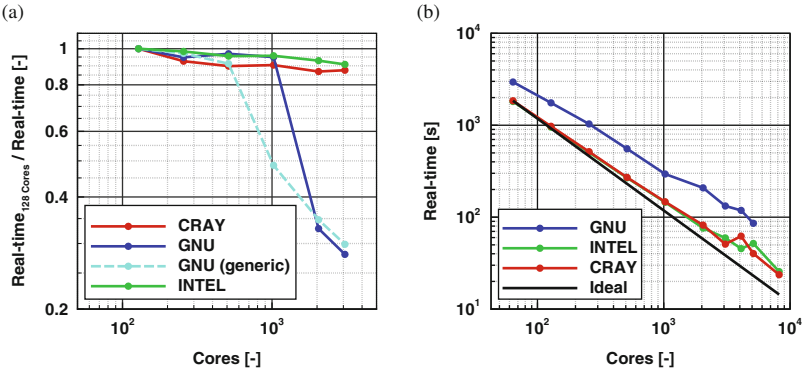

Fig. 10 CRAY-/GNU-/INTEL-compiled version of TAU code version 2.2.0. (**a**) Weak scaling test; Smallest 'Real'-time results out of three test runs. (**b**) Strong scaling test

All versions of the code indicate differences in some points dependent on the allocated compute nodes. An extreme value of approx. 65 % deviation was found for the CRAY-compiled version and 3072 nodes. A second extreme value of approx. 105 % deviation is observable for the GNU-compiled version and 1024 nodes.

To compare the scaling behavior of all three compilers, the smallest values out of the three mentioned test runs are plotted against the number of nodes in Fig. 10a. All measured data points are normalized with the test result of 128 nodes, respectively. Analyzing the chart, the scaling behavior of the GNU-compiled version of TAU indicates major differences towards the CRAY-/INTEL-compiled code versions for high numbers of compute nodes (2048/3072). Those results are not an isolated case. As shown in Fig. 9b, all runs indicate a major increase of 'real-time' for 2048 and 3072 nodes. Even a second measurement series applying a GNU-compiled code version with slightly different compiler flags validates the presented results of the GNU-compiled code. Besides the mentioned observations, the INTEL compiler shows the best scaling efficiency followed by the CRAY compiler. The GNU compiler indicates values almost as good as the INTEL compiler, but only in the range of 128 till 1024 nodes. Apart from the extreme values given by the

GNU compiler at high node numbers, the worst scaling factor in this particular test amounts to 87.6 %.

For the strong scaling test, on the other hand, the mesh of 33.5 mio cells was divided into a range of different domain numbers. The first test results are obtained using 64 cores, which equals 2,097,152 cells per domain. Under certain circumstances, a core number higher than 5120 caused problems using the parallel in-code partitioner presumably because of the cell number per domain is less than 7000. This issue might be exacerbated when using high-order multi-grid schemes, which further reduce the cell number per domain. Furthermore, queuing duration is many times higher than simulation time, making this approach inefficient. Figure 10b depicts the 'Real-time' plotted against the number of cores for the three compilers. The TAU Code shows good linear behavior within a wide range of cores for all versions, followed by a deviation in the results of the INTEL and CRAY compiler. In the linear region the results for INTEL and CRAY overlap. For the CRAY compiler the deviation starts at 3072 cores while the INTEL compiler remains linear up to 4096 cores. Those results were reproducible in three separate runs. Interestingly, for a core number of 5120 domains, the results seem to meet the linear behavior again. The GNU results show a similar gradient but experience a time offset compared to the other compilers, meaning it takes longer to complete for any number of cores. The ideal results for the CRAY compiler depicted in Fig. 10b need parallel translation for the GNU results. The gradients of the results slightly differ from the ideal results, presumably due to processing overhead required for each additional core. This means, increasing the number of cores reduces the simulation time but increases the overall numerical costs. In order to get the most economic results a compromise between overall numerical cost and simulation time has to be found.

7 Conclusions

Originally designed for (wave) drag reduction in transonic flight, it has been shown that shock control bumps (SCB) can also alleviate buffet, an unsteady shock motion due to continuous flow separation and re-attachment at the rear part of the airfoil. Analyzing the effect of flank shape of a three-dimensional wedge-like SCB on performance and buffet behavior, this paper presents a parametric study on different flank configurations. Reference configuration is the OALT25 airfoil equipped with a performance optimized SCB (using RANS simulations), reducing (wave) drag at its design point considerably. By modifying front and rear flank shape of the bump, URANS simulations predict an improved buffet behavior. It was found that longer flanks are beneficial for both, performance at airfoil off-design condition and buffet behavior. Concerning width of the flanks, a narrow front and wide rear flank improve maximum lift coefficient and alleviate lift oscillations at buffet onset. Important for up-coming bump optimization, it was found that both, maximum span-wise pressure gradient as well as flow separation on the bump are suitable design objectives.

Acknowledgements This study is undertaken within the European-Russian project BUTERFLI, supported by the European FP7 program (FP7-AAT-2013.8-1-RTD-RUSSIA) under Grant Agreement no. 605605.

References

1. Ashill, P., Fulker, J., Shires, A.: A novel technique for controlling shock strength of laminar-flow aerofoil sections. In: Proceedings: 1st European Forum on Laminar Flow Technology (1992)
2. Bogdanski, S.: Numerische Untersuchungen zum stoßinduzierten Buffet. Verlag Dr. Hut, München (2014)
3. Bogdanski, S., Nübler, K., Lutz, T., Krämer, E.: Numerical investigation of the influence of shock control bumps on the buffet characteristics of transonic airfoils. In: New Results in Numerical and Experimental Fluid Mechanics IX, 124 edn., Springer International Publishing (2014)
4. Bogdanski, S., Gansel, P., Lutz, L., Krämer, E.: Impact of 3d shock control bumps on transonic buffet. In: High Performance Computing in Science and Engineering '14, pp. 447–461. Springer International Publishing (2015)
5. Bruce, P.J.K., Colliss, S.P.: Review of research into shock control bumps. Shock Waves **25**(5), 451–471 (2015)
6. Bruce, P.J.K., Colliss, S.P., Babinsky, H.: Three-dimensional shock control bumps: effects of geometry. In: 52nd AIAA Aerospace Sciences Meeting, pp. 1–17 (2014)
7. Colliss, S.P., Babinsky, H., Nübler, K., Lutz, T.: Vortical structures on three-dimensional shock control bumps.In: 51st AIAA Aerospace Sciences Meeting including the New Horizons Forum and Aerospace Exposition, January (2013)
8. DLR. Tau-code userguide 2014.2.0. 16.09.2014
9. Drela, M., Giles, M.B.: Viscous-inviscid analysis of transonic and low Reynolds number airfoils. AIAA J. **25**(10), 1347–1355 (1987)
10. Eastwood, J.P., Jarrett, J.P.: Toward designing with three-dimensional bumps for lift/drag improvement and buffet alleviation. AIAA J. **50**, 2882–2898 (2012)
11. Illi, S.A., Lutz, T.: Transonic tail buffet simulations on the ATRA research aircraft. Comput. Flight Testing **123**, 273–287 (2013)
12. Jacquin, L., Molton, L., Deck, S., Maury, B., Soulevant, D.: Experimental study of shock oscillation over a transonic supercritical profile. AIAA J. **47**, 1985–1994 (2009)
13. König, B., Pätzold, M., Lutz, T., Krämer, E., Rosemann, H., Richter, K., Uhlemann, H.: Numerical and experimental validation of three-dimensional shock control bumps. J. Aircr. **46**(2), 675–682 (2009)
14. Nuebler, K., Colliss, S.P., Lutz, T., Babinsky, H.: Numerical and experimental examination of shock control bump flow physics. In: High Performance Computing in Science and Engineering 2012, pp. 333–349. Springer, Berlin (2013)
15. Rossow, C., Kroll, N., Schwamborn, D.: The MEGAFLOW project - numerical flow simulation for aircraft. In: Progress in Industrial Mathematics at ECMI 2004, pp. 3–33, 8th edn. Springer, Berlin/Heidelberg (2006)
16. Schulz, C., Fischer, A., Weihing, P., Lutz, T., Krämer, E.: Evaluation and control of loads on wind turbines under different operating conditions by means of cfd. High Performance Computing in Science and Engineering '15 (2015, submitted)
17. Soda, A.: Numerical investigation of unsteady transonic shock/boundary-layer interaction for aeronautical applications. Ph.D. thesis, Technical University of Aachen (2006)